

Ref #	Hits	Search Query	DBs	Default Operator	Plurals	Time Stamp
L1	0	"aluminum nitride tantalum nitride"	USPAT	OR	OFF	2005/10/07 10:39
L2	0	"aluminum nitride tantalum nitride"	US-PGPUB; USPAT	OR	OFF	2005/10/07 10:40
L3	0	AlNTaN	US-PGPUB; USPAT	OR	OFF	2005/10/07 10:40
L4	1789	"tantalum nitride" and "power supply"	US-PGPUB; USPAT	OR	OFF	2005/10/07 10:41
L5	1527	4 and (electrode cathode anode susceptor holder)	US-PGPUB; USPAT	OR	OFF	2005/10/07 10:46
L6	15	"ootsuka takeshi" "endou kazunori"	US-PGPUB; USPAT	OR	OFF	2005/10/07 10:54
L7	0	"aluminum nitride tunsten"	US-PGPUB; USPAT	OR	OFF	2005/10/07 10:55
L8	0	aluminum with nitride with tunsten	US-PGPUB; USPAT	OR	OFF	2005/10/07 10:55

Full Text: [[PDF \(558 kB\)](#) [GZipped PS](#)] [Order](#)

Citing Articles

This list contains links to other [online articles](#) that cite the article currently being viewed.

1. Cu Wettability and Diffusion Barrier Property of Ru Thin Film for Cu Metallization
[Hoon Kim *et al.*, J. Electrochem. Soc. **152**, G594 \(2005\)](#)
2. Robust TaN_x diffusion barrier for Cu-interconnect technology with subnanometer thickness by metal-organic plasma-enhanced atomic layer deposition
[H. Kim *et al.*, J. Appl. Phys. **98**, 014308 \(2005\)](#)
3. Process integration for through-silicon vias
[S. Spiesshoefer *et al.*, J. Vac. Sci. Technol. A **23**, 824 \(2005\)](#)
4. Comparative study of polycrystalline Ti, amorphous Ti, and multiamorphous Ti as a barrier film for Cu interconnect
[Keng-Liang Ou *et al.*, J. Vac. Sci. Technol. B **23**, 229 \(2005\)](#)
5. Numerical and Experimental Analysis of Cu Diffusion in Plasma-Treated Tungsten Barrier
[Kou-Chiang Tsai *et al.*, J. Electrochem. Soc. **152**, G83 \(2005\)](#)
6. Chemically enhanced physical vapor deposition of tantalum nitride-based films for ultra-large-scale integrated devices
[Ning Li *et al.*, J. Vac. Sci. Technol. B **22**, 2734 \(2004\)](#)
7. High Cu Diffusion Resistance in Ultrathin Multiquasi-amorphous CVD-Ti/TiN_x Films
[Keng-Liang Ou *et al.*, J. Electrochem. Soc. **151**, G766 \(2004\)](#)
8. Failure Mechanism of Amorphous and Crystalline Ta-N Films in the Cu/Ta-N/Ta/SiO₂ Structure
[Ching-Chun Chang *et al.*, J. Electrochem. Soc. **151**, G746 \(2004\)](#)
9. Nanostructured TaN(O)/TaN Barrier Film Formed by Oxygen Plasma Treatment for Copper Interconnect
[Keng-Liang Ou *et al.*, Electrochem. Solid-State Lett. **7**, G272 \(2004\)](#)
10. Effectiveness of reactive sputter-deposited Ta-N films as diffusion barriers for Ag metallization
[Daniel Adams *et al.*, J. Vac. Sci. Technol. B **22**, 2345 \(2004\)](#)
11. The physical properties of cubic plasma-enhanced atomic layer deposition TaN films
[H. Kim *et al.*, J. Appl. Phys. **95**, 5848 \(2004\)](#)
12. Characterization of Atomic Layer Deposited WN_xC_y Thin Film as a Diffusion Barrier for Copper Metallization
[Soo-Hyun Kim *et al.*, J. Electrochem. Soc. **151**, C272 \(2004\)](#)
13. Preferred orientation and film structure of TaN films deposited by reactive magnetron sputtering
[Suguru Noda *et al.*, J. Vac. Sci. Technol. A **22**, 332 \(2004\)](#)
14. Effect of the substrate bias voltage on the physical characteristics of copper films deposited by microwave plasma-assisted sputtering technique
[F. Thiéry *et al.*, J. Vac. Sci. Technol. A **22**, 30 \(2004\)](#)
15. Growth and characteristics of TaN/TiN superlattice structures
[H. Wang *et al.*, Appl. Phys. Lett. **83**, 3072 \(2003\)](#)
16. Deposition pressure dependence of internal stress in TiN films deposited by filtered cathodic vacuum arc
[Y. H. Cheng *et al.*, J. Vac. Sci. Technol. A **21**, 1609 \(2003\)](#)
17. Multilayer diffusion barrier for copper metallization using a thin interlayer metal (M = Ru, Cr, and Zr) between two TiN films
[Soo-Hyun Kim *et al.*, J. Vac. Sci. Technol. B **21**, 804 \(2003\)](#)

18. Effects of Nitrogen Plasma Treatment on Tantalum Diffusion Barriers in Copper Metallization
Wen-Fa Wu *et al.*, J. Electrochem. Soc. **150**, G83 (2003)
19. Effect of pH and H₂O₂ on Ta Chemical Mechanical Planarization
S. C. Kuiry *et al.*, J. Electrochem. Soc. **150**, C36 (2003)
20. The Effect of NH₃ Plasma Treatment on the Electroless Copper Deposition on TaN_x (x = 0 = 1)
Diffusion Barriers.
Seok Woo Hong *et al.*, Electrochem. Solid-State Lett. **6**, C12 (2003)
21. Improved TaN barrier layer against Cu diffusion by formation of an amorphous layer using
plasma treatment
Keng-Liang Ou *et al.*, J. Vac. Sci. Technol. B **20**, 2154 (2002)
22. Electrical properties of TiN films deposited by filtered cathodic vacuum arc
Y. H. Cheng *et al.*, J. Vac. Sci. Technol. B **20**, 2000 (2002)
23. Copper diffusion characteristics in single-crystal and polycrystalline TaN
H. Wang *et al.*, Appl. Phys. Lett. **81**, 1453 (2002)
24. Ta and Ta-N diffusion barriers sputtered with various N₂/Ar ratios for Cu metallization
J. H. Wang *et al.*, J. Vac. Sci. Technol. B **20**, 1522 (2002)
25. Thin-film resistor fabrication for InP technology applications
R. F. Kopf *et al.*, J. Vac. Sci. Technol. B **20**, 871 (2002)

[See more Citing Articles...](#)

Full Text: [[PDF \(558 kB\)](#) [GZipped PS](#)] [Order](#)

[[Previous](#) / [Next Abstract](#) | [Issue Table of Contents](#) | [Top of Page](#)]

SEARCH	SPIN Web	Search SPIN	BROWSE
Current Issue	Browse SPIN	Advanced Abstracts	Accelerated Articles
Issue Archive	© 2005 AVS The Science & Technology Society		Current Issue
			Issue Archive

Comparative study of tantalum and tantalum nitrides (Ta_2N and TaN) as a diffusion barrier for Cu metallization*

Kyung-Hoon Min, Kyu-Chang Chun, and Ki-Bum Kim

Department of Metallurgical Engineering, Inter-university Semiconductor Research Center, Seoul National University, Seoul, Korea

(Received 7 November 1995; accepted 13 July 1996)

Tantalum (Ta) and tantalum nitride films (Ta_2N and TaN) of about 50 nm thickness were reactively sputter deposited onto (100) Si substrate by using dc magnetron sputtering and their diffusion barrier properties in between Cu and Si were investigated by using sheet resistance measurement, x-ray diffraction, Auger electron spectroscopy, and Secco etching. With increasing amounts of nitrogen in the sputtering gas, the phases in the as-deposited film have been identified as a mixture of β -Ta and bcc-Ta, bcc-Ta, amorphous Ta_2N , and crystalline fcc-TaN. Diffusion barrier tests indicate that there are two competing mechanisms for the barrier failure; one is the migration of Cu into the Si substrate and another is the interfacial reaction between the barrier layer and the Si substrate. For instance, we identified that elemental Ta barrier failure occurs initially by the diffusion of Cu into the Si substrate through the barrier layer at 500 °C. On the other hand, the Ta_2N barrier fails at 700 °C by the interfacial reaction between Ta_2N and Si substrate instead of the migration of Cu into the Si substrate. For the case of TaN, the barrier failure occurs by the migration of Cu into the Si substrate at 750 °C. It is also demonstrated that the diffusion barrier property is enhanced as the nitrogen concentration in the film is increased. © 1996 American Vacuum Society.

I. INTRODUCTION

Copper has drawn much attention as a new interconnect material for deep submicron integrated circuits (ICs) as a replacement for Al and its alloys. The major motivation for this replacement is due to the lower resistivity and superior electromigration and stress migration resistance of Cu as compared to Al and its alloys.^{1,2} However, in order to successfully integrate Cu metallization into ICs, some problems associated with the transition to Cu such as lack of an anisotropic etching, oxidation, corrosion, and poor adhesion to most of the dielectric layers should be resolved. In particular, the diffusion of Cu into either Si and SiO_2 layers should be retarded by employing a suitable diffusion barrier layer.^{3,4}

Indeed, there has been a considerable effort to identify a suitable diffusion barrier layer for Cu metallization. Materials investigated include Ta ,⁵⁻⁸ W ,⁹ TiW ,¹⁰ TiSi_2 ,¹¹ TiN ,^{12,13} Ta_2N ,⁵ W_2N ,¹⁴ $\text{Ni}_{0.6}\text{Nb}_{0.4}$,¹⁵ and amorphous Ta-Si-N.⁸ The results of these efforts has been well summarized recently by Wang.¹⁶ Among these materials, tantalum has been extensively investigated as a diffusion barrier for Cu since it not only shows relatively high melting temperature but is also known to be thermodynamically stable with respect to Cu.¹⁷ For instance, Holloway *et al.*⁵ and Catania *et al.*⁶ investigated the barrier properties of sputter deposited 50-nm-thick Ta layer and identified that the layer was stable up to 550 and 650 °C, respectively. In contrast, Chang⁷ observed intermixing of Cu and Si through the Ta barrier layer even at 300 °C by Rutherford backscattering spectroscopy (RBS). In addition, Kolawa *et al.*⁸ identified that the junctions covered with a 180-nm-thick Ta barrier layer and Cu failed after annealing at 500 °C for 30 min. Thus, it appears that there still is a controversy about the barrier failure temperature of Ta.

In particular, we note that the barrier failure temperature is quite different depending on the method to identify the barrier failure. In addition, we note that there are only few reports describing the barrier properties of tantalum nitrides such as Ta_2N and TaN. Holloway *et al.*⁵ reported that 50-nm-thick Ta_2N was stable up to 650 °C, thus indicating that the barrier property was improved by about 100 °C compared to that of pure Ta film. However, as far as we are aware of, the effectiveness of TaN as a diffusion barrier between Cu and Si has not been reported so far.

In this article, we would like to systematically investigate the diffusion barrier properties of Ta and its nitrides, both Ta_2N and TaN, for Cu metallization and identify the barrier failure mechanism in each cases. In order to do this, we first reactively sputter deposited the films at various N_2/Ar ratios and identified the phases and microstructure of the as-deposited film. Then, the barrier properties of the Ta, Ta_2N , and TaN films were tested.

II. EXPERIMENTS

Tantalum and tantalum nitride films of about 50 nm thickness were deposited onto (100) Si substrates by using dc magnetron sputtering at various N_2/Ar gas ratios. Si wafers were cleaned in 10:1 diluted HF solution and rinsed in deionized water before loading into the chamber. During deposition, the operating pressure was maintained at 10 mTorr and the substrates were water cooled. The phases and microstructures of the as-deposited films were investigated by x-ray diffractometry (XRD) and plan-view transmission electron microscopy (plan-view TEM) operated at 200 kV and the nitrogen content of the as-deposited films was obtained by using RBS and Auger electron spectroscopy (AES).

In order to identify the barrier properties, 300-nm-thick Cu layer was deposited on top of the barrier layer without

*Published without author corrections

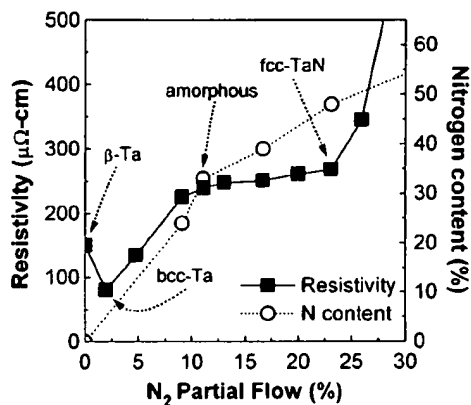


FIG. 1. The electrical resistivity and the nitrogen content of the films deposited at various N_2/Ar gas ratios.

breaking the vacuum and the samples were annealed for one hour at the temperatures ranging from 400 to 750 °C in hydrogen ambient. Sheet resistance of the samples were measured both before and after annealing by four-point probe to survey the overall reaction involving Cu. XRD and AES were used for the analysis of reaction product phases and the interdiffusion of the elements across the interface, respectively. Finally, Secco etching of the substrates was performed to identify the Cu penetration into the Si substrate after removing both Cu and barrier layers by wet-chemical solution.^{18,19} The wet-chemicals used in this experiment are $HNO_3:H_2O=1:20$ for Cu, $HF:H_2O=1:10$ for Ta, and $H_2SO_4:HF=9:1$ for both Ta_2N and TaN. The Si substrates were then Secco etched and examined by using optical microscopy.

III. EXPERIMENTAL RESULTS AND DISCUSSION

A. The microstructure and phases of the as-deposited films

Both electrical resistivity and nitrogen content of the films deposited at various N_2/Ar gas ratios are shown in Fig. 1. It shows that the nitrogen content in the film is gradually increased as the partial flow of nitrogen in the sputtering gas is increased. The resistivity of the as-deposited film, however, shows several interesting features. It first shows that the electrical resistivity of the pure Ta film is about 150 $\mu\Omega$ cm and is initially decreased to about 80 $\mu\Omega$ cm as small amount of nitrogen is added to the sputtering gas. Then, the value of the resistivity gradually increased up to about 220 $\mu\Omega$ cm as the nitrogen content in the film is increased to about 24 at. %. In between the nitrogen content of about 24 to 48 at. %, the resistivity of the film is only slightly increased from about 220 to about 260 $\mu\Omega$ cm. Finally, when further nitrogen is incorporated, the resistivity of the film drastically increased. The oxygen concentrations of pure Ta film, 24 at. % N contained film, and 48 at. % N contained film are almost the same. All the films contain about 1–2 at. % oxygen.

In order to clearly understand the relationship between the resistivity and the nitrogen content in the film, both the

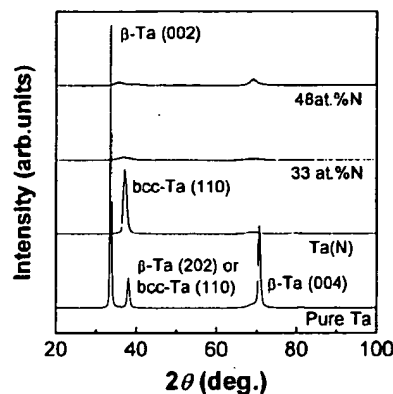


FIG. 2. XRD patterns of the as-deposited Ta–N films deposited at various N_2/Ar flow ratios. The numbers inside of the parentheses indicated the nitrogen content in the film measured by RBS.

phase(s) and the microstructure of the films have been investigated by using XRD and plan-view TEM. First, Fig. 2 shows the XRD patterns of Ta–N films containing various amount of nitrogen. The XRD peaks of the pure Ta film can be indexed as (002) and (004) of β -Ta except the one appearing at 38°, which can also be indexed as (202) of β -Ta or (110) of bcc-Ta. Thus, it is not clear from XRD whether the film only contains β -Ta or is a mixture of bcc-Ta and β -Ta. The XRD pattern of Ta(N) film deposited with 3% partial N_2 shows only one peak at 38°, which can be ascribed to either (110) of bcc-Ta or (202) of β -Ta. These results indicate that the addition of a small amount of N_2 in the sputtering gas either induce a phase transformation from β -Ta to bcc-Ta or induce the texture of the β -Ta film to change. For the films with higher nitrogen content, it is difficult to identify the phase(s) of the film by using XRD since only one or two weak and broad peaks appear.

To further determine the phase(s) in the as-deposited films, the films were analyzed using plan-view TEM. Figure 3 shows a series of bright field images and selected area diffraction (SAD) patterns of the as-deposited films with different amounts of nitrogen contents in the film. First, the bright field image and SAD of the pure Ta film clearly show that the film is composed of a mixture of β -Ta and bcc-Ta, with a grain size of about 20 to 30 nm [Fig. 3(a)]. Thus, from the results of XRD and TEM, we can conclude that the pure Ta film consists of a mixture of β -Ta and bcc-Ta. Moreover, the β -Ta phase in the film is observed to form a strong (002) texture, while the bcc-Ta phase in the film forms a (110) texture. Figure 3(b) shows the bright field image and SAD pattern of the films deposited with 3% of N_2 in the sputtering gas. The SAD pattern of this sample clearly shows that the film only contains bcc-Ta and the bright field image shows that the grain size of this film is similar to that of pure Ta film. Figure 3(c) shows both the TEM image and SAD pattern of the Ta–N film with 33 at. % of nitrogen in the film which shows that the film forms an amorphous phase. Finally, Fig. 3(d) is the bright field image and SAD of the TaN film showing the formation of a crystalline fcc phase with

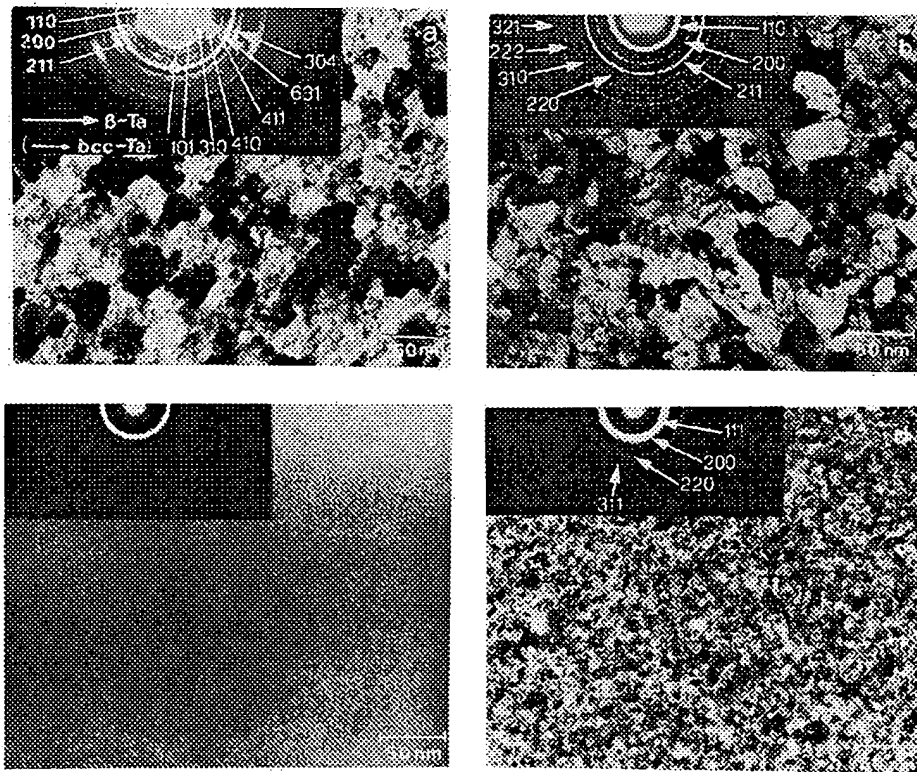


FIG. 3. Plan-view TEM micrographs and selected area diffraction patterns of the as-deposited films: (a) pure-Ta; (b) Ta(N); (c) Ta₂N; and (d) TaN.

grains having sizes of a few nm. Interplanar spacings derived from the SAD pattern agree with those of TaN.

If one reviews the results of resistivity and phase identification, the initial decrease of the resistivity from about 150 $\mu\Omega$ cm to about 80 $\mu\Omega$ cm with small N₂ addition can be ascribed to the phase transformation from β -Ta to bcc-Ta. Indeed, it has been well known the typical reported resistivities of β -Ta are about 180 $\mu\Omega$ cm, and for bcc-Ta about 40 $\mu\Omega$ cm.^{20,21} Although it is not clear yet why this phase transformation occurs by the addition of small amounts of nitrogen in the sputtering gas, similar behavior has been reported by others.^{18,20–25} It is also interesting to note that an amorphous phase is formed at about 33 at. % nitrogen content [Fig. 3(c)]. Reid *et al.*²⁶ reported the formation of a mixture of amorphous and crystalline Ta₂N phase close to this composition. In contrast, Holloway *et al.*⁵ reported the formation of a crystalline Ta₂N phase. The formation of a mixture of amorphous and crystalline Ta₂N phase is also observed in our case. Therefore, at somewhat smaller concentration of nitrogen, it appears that the formation of amorphous, crystalline, or mixtures of amorphous and crystalline Ta₂N phase is all possible. It is believed that small variations of N content or the sputtering parameters can explain the different observations.

B. Barrier properties

Having discussed the evolution of microstructure and phase(s) of the film by varying the nitrogen content, we now

turn our attention to the diffusion barrier properties of each of these films. Figure 4 shows the variation of the sheet resistance of the samples upon annealing. The data mainly show changes in the thickness or resistivity of the unreacted Cu layer, since the sheet resistance of the barrier layer and reaction products are expected to be much larger than that of Cu. We first note that the sheet resistance of the film stack initially drops by annealing which apparently is caused by a decrease in defect density and grain growth in the Cu film. The sheet resistance of the Cu/Ta/Si film increased slightly

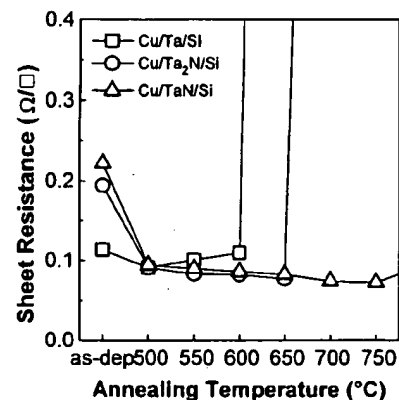


FIG. 4. Sheet resistance variation of the Cu/Ta/Si, Cu/amorphous Ta₂N/Si, and Cu/TaN/Si samples as a function of annealing temperature.

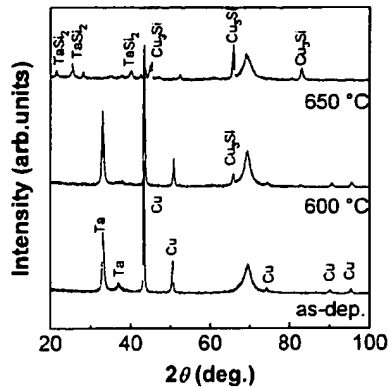


FIG. 5. XRD patterns of the Cu/Ta/Si sample after annealing at various temperatures: (a) as-deposited; (b) 600 °C; and (c) 650 °C.

upon annealing at 600 °C. However, after annealing at 650 °C, the color of the sample is observed to change from Cu color to gray, and the sheet resistance of the sample can be observed to drastically increase, which indicates that a significant reaction has now occurred in between the layers. A similar behavior occurs at 700 °C for Cu/Ta₂N/Si samples while no such behavior occurs for the Cu/TaN/Si samples even after annealing at 750 °C.

Figure 5 shows the XRD results of the Cu/Ta/Si sample after annealing. It clearly shows the formation of Cu₃Si at 600 °C and the formation of Cu₃Si and TaSi₂ at 650 °C. These results are similar to those of Holloway *et al.*⁵ who also identified the abrupt increase of the sheet resistance with the formation of Cu₃Si and TaSi₂. XRD results of Cu/Ta₂N/Si samples (Fig. 6) show that the crystallization of amorphous Ta₂N film occurs at about 500 °C, and the formation of Cu₃Si and TaSi₂ after annealing at 700 and 750 °C, respectively. The crystallization temperature of amorphous Ta₂N reported here (500 °C) appears to be a little bit lower than that of Sun *et al.*,²⁷ who reported that a mixture of amorphous and crystalline Ta₂N film crystallized after annealing at 600 °C for 65 min. It appears that there is still a

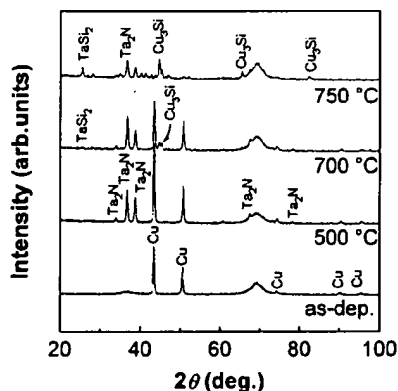


FIG. 6. XRD patterns of the Cu/amorphous Ta₂N/Si sample after annealing at various temperatures: (a) as-deposited; (b) 500 °C; (c) 700 °C; and (d) 750 °C.

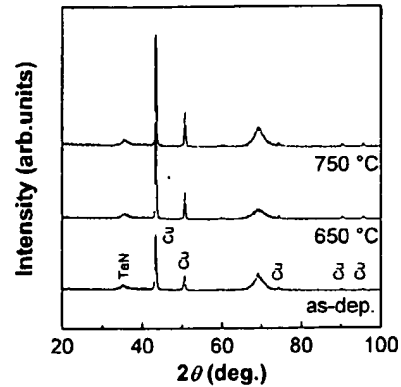


FIG. 7. XRD patterns of the Cu/crystalline fcc-TaN/Si sample as a function of annealing temperature: (a) as-deposited; (b) 650 °C; and (c) 750 °C.

controversy on the role of Cu in crystallization process of some amorphous films. For instance, Reid *et al.*²⁶ suggested that Cu reduces the crystallization temperature of some amorphous films. However, Thomas *et al.*²⁸ reported that a

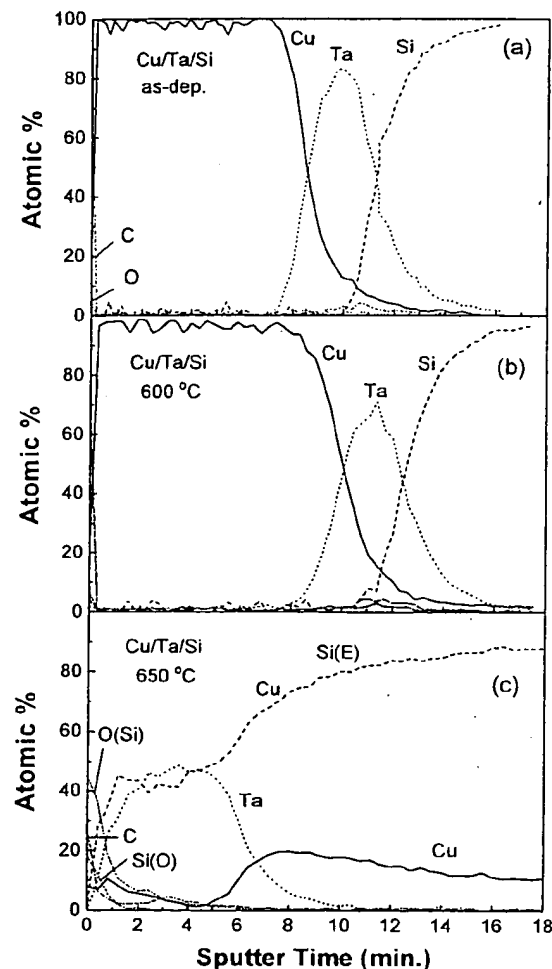


FIG. 8. AES depth profiles of the Cu/Ta/Si samples: (a) as-deposited; (b) 600 °C, 1 h annealing; and (c) 650 °C, 1 h annealing.

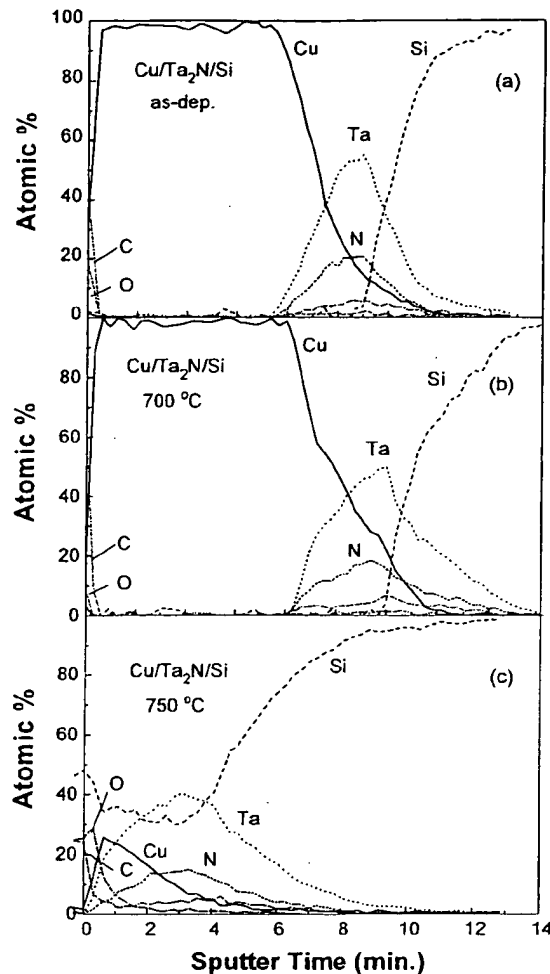


FIG. 9. AES depth profiles of the Cu/amorphous $\text{Ta}_2\text{N}/\text{Si}$ samples: (a) as-deposited; (b) 700, 1 h annealing; and (c) 750 °C, 1 h annealing.

Cu overlayer had little effect on reducing the crystallization temperature of amorphous W-Si film, while an Al overlayer significantly reduces the crystallization temperature. In order to check the effect of Cu on the crystallization temperature of amorphous Ta_2N phase, a Ta_2N film without Cu overlayer has been annealed. It is observed that the crystallization of amorphous Ta_2N occurs at the same temperature, irrespective of the presence of a Cu layer. Finally, Fig. 7 shows the XRD results of the Cu/TaN/Si film which shows no indication of reaction even after annealing at 750 °C.

Additional results have been obtained in the AES depth profiling. In Fig. 8, we note that Cu diffuses deep into the Si substrate after annealing at 650 °C. It also shows that extensive intermixing of Ta and Si has occurred at the surface. Figure 9 shows the AES depth profiles of the Cu/amorphous $\text{Ta}_2\text{N}/\text{Si}$ sample. The barrier failure mode is different compared to that of the pure Ta (Fig. 8). Figure 9 shows that Cu still remain at the surface even though the Ta and Si signal significantly intermixed after annealing at 750 °C. This result clearly demonstrates that diffusion of Cu into the Si substrate

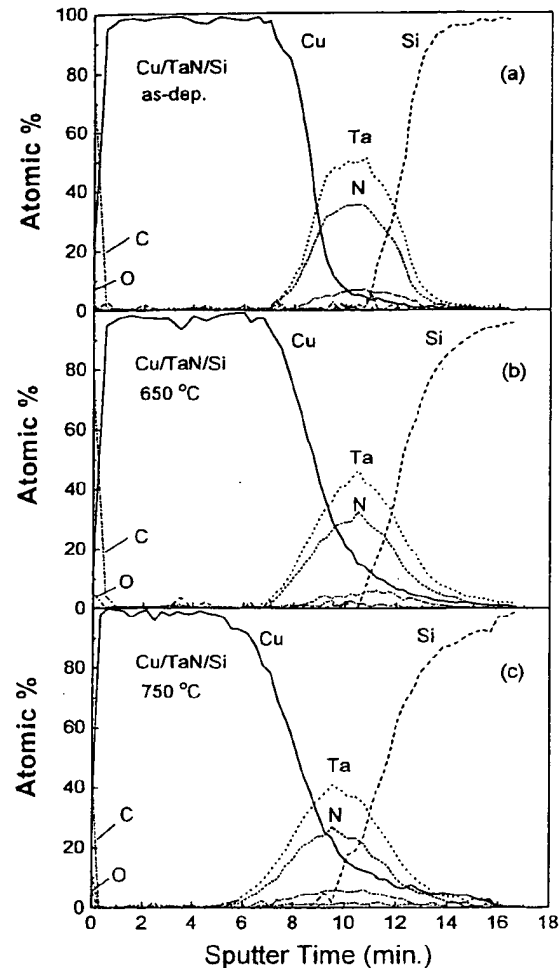


FIG. 10. AES depth profiles of the Cu/TaN/Si samples: (a) as-deposited; (b) 650 °C, 1 h annealing; and (c) 750 °C, 1 h annealing.

is significantly slower in the case of a Ta_2N layer than it is in the case of a Ta. Finally, Fig. 10 shows a series of AES depth profiles of the Cu/TaN/Si diffusion couple. As is expected from the XRD results, no significant intermixing occurs even after annealing at 750 °C. The evaluation of barrier properties using AES depth profile has two shortcomings in our case. One is that the profiles of as-deposited films do not show abrupt slope at the interface due to nonuniform etching of film during AES depth profile. The other is roughness of annealed Cu film surface caused by grain growth during heat treatment, which makes the profiles of annealed samples worse than that of as-deposited one.

The Si surface of annealed samples was also examined by using optical microscopy after Secco etching (Fig. 11). In case of Cu/Ta/Si sample, we first observed the formation of etch pits on samples annealed at 500 °C. Both the size and the density of etch pits increase with the annealing temperature as is shown in Fig. 12. Using cross-sectional TEM, Park and Kim¹³ noted that the initial failure of the Cu/TiN/Si sample occurs by the diffusion of Cu into the Si substrate

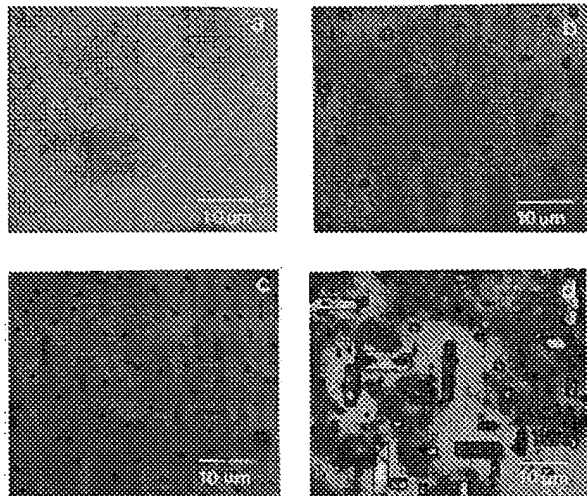


FIG. 11. A series of optical micrographs showing the surface of Si after Secco etching: (a) 450 °C, 1 h annealing; (b) 500 °C, 1 h annealing; (c) 550 °C, 1 h annealing; and (d) 600 °C, 1 h annealing.

which resulted in the formation of the crystalline defects (dislocations) decorated with small size of Cu_3Si precipitates. From the previous work, it is concluded that the formation of etch pits by Secco etching is related to the formation of these defects in the Si substrate. It should be noted that the formation of reaction product phase(s) is first identified by XRD at 600 °C while the formation of etch pits is first observed at 500 °C. This result indicates that the etch pit observation is a more sensitive technique to identify barrier failure temperatures than either XRD or AES. On $\text{Cu}/\text{Ta}_2\text{N}/\text{Si}$ samples, the formation of etch pits is not observed even after annealing at 650 °C. For samples annealed at temperature higher than 650 °C, the formation of etch pits is not observed since a significant reaction now has occurred at the $\text{Ta}_2\text{N}/\text{Si}$ interface (as is shown from the results of XRD and AES). From these results, we can conclude that the Ta_2N barrier is good enough to protect the migration of Cu into the Si substrate at least up to 650 °C. The barrier failure, in this

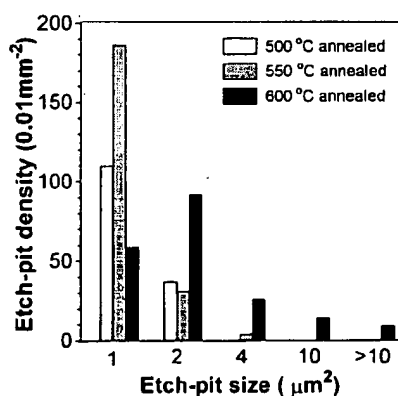


FIG. 12. Etch pit density of the $\text{Cu}/\text{Ta}/\text{Si}$ sample as a function of annealing temperature.

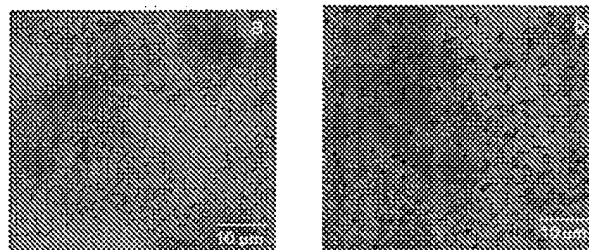


FIG. 13. Optical micrographs of the Si surface after Secco etching: (a) $\text{Cu}/\text{Ta}_2\text{N}/\text{Si}$ sample after annealing at 650 °C and (b) $\text{Cu}/\text{Ta}_2\text{N}/\text{Si}$ sample after annealing at 750 °C.

case, occurs by the interfacial reactions between Ta_2N and Si. The $\text{Cu}/\text{Ta}_2\text{N}/\text{Si}$ sample demonstrates a clean surface even after annealing at 700 °C. Etch pits are first observed in the samples annealed at 750 °C as is shown in Fig. 13. The interface between TaN and Si is quite stable even up to 800 °C. Due to the strong thermal stability of this interface, the ultimate failure of the diffusion barrier occurs by the migration of Cu into the Si substrate.

Our results thus indicate that the barrier failure of the tantalum and its nitrides occurs by two different mechanisms. One is the diffusion of Cu into the Si substrate through the barrier layer which resulted in the formation of crystalline defects and Cu_3Si precipitates in the Si substrates. This is the predominant failure mechanism for $\text{Cu}/\text{Ta}/\text{Si}$ and $\text{Cu}/\text{Ta}_2\text{N}/\text{Si}$ samples. The other mechanism is by the chemical reactions between the barrier layer and the Si substrate as is demonstrated in the $\text{Cu}/\text{Ta}_2\text{N}/\text{Si}$ samples. According to the Cu-Ta-N ternary phase diagram shown in Fig. 14(a), Cu is thermodynamically stable with respect to Ta, Ta_2N , and TaN. However, the ternary phase diagram drawn from the Gibbs free energy data at 900 °K [Fig. 14(b)] shows that both tantalum and its nitrides (Ta_2N and TaN) are thermodynamically not stable with respect to Si. However, our results suggest that the interfacial reaction between TaN and Si occurs at much higher temperature than that of between Ta_2N and Si. For this reason, the barrier failure of Ta_2N occurs by the interfacial reaction while the barrier failure of TaN occurs by the diffusion of Cu through the barrier layer.

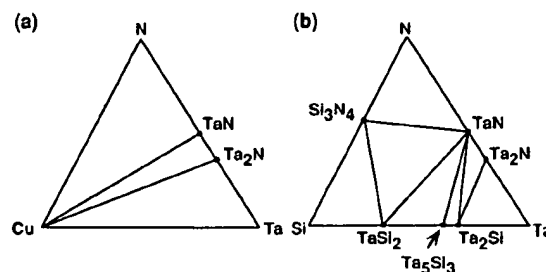


FIG. 14. Isothermal section of a ternary phase diagram of (a) Cu-Ta-N and (b) Ta-N-Si systems drawn at 900 K.

IV. CONCLUSION

We have investigated the evolution of the microstructure and phase(s) of the Ta-N systems by varying the nitrogen content in the film. It is identified that the as-deposited pure Ta film forms a mixture of β -Ta and bcc-Ta with a grain size of about 20 to 30 nm. When a small amount of nitrogen is incorporated in the sputtering gas, the phase changes from a mixture of β -Ta and bcc-Ta to pure bcc-Ta without a change in grain size. It is also identified that both amorphous and a mixture of amorphous and crystalline Ta₂N phase can be formed when the nitrogen content in the film is around 33 at. % and the crystalline fcc-TaN phase is formed when the nitrogen content in the film is from about 40 to 48 at. %.

By using sheet resistance measurements, XRD, AES depth profiles, and etch pit observations after Secco etching, it is identified that the diffusion barrier property is significantly enhanced as the nitrogen content in the film is increased. Importantly, we note that there are two different mechanisms of barrier failure; one is by the migration of Cu into the Si substrate by diffusion through the barrier layer and the other is the interfacial reactions between the barrier layer and the Si substrate. Ta apparently fails initially by the diffusion of Cu into the Si substrate at 500 °C and by the formation of CuSi₃ and TaSi₂ at higher temperatures. On the other hand, for the case of Ta₂N film, the barrier failure occurs at around 700 °C by the chemical reaction between Ta₂N and Si. Finally, the TaN film, deposited as an fcc crystalline phase, is identified as a stable barrier up to 700 °C and the barrier failure occurs by the migration of Cu into the Si substrate.

ACKNOWLEDGMENTS

This research was funded in part by the Ministry of Education through the Inter-University Semiconductor Research Center at Seoul National University (IRS-94-E-1017) and in part by the Ministry of Science and Technology of Korea

through Electrical Telecommunication Research Institute (ETRI). The authors are also grateful to Dr. Moshe Eizenberg and Dr. Ivo Raaijmakers at Applied Materials, Inc. for the critical review of this manuscript.

- ¹T. Nitta, T. Ohmi, T. Hoshi, S. Sakai, K. Sakaibara, S. Imai, and T. Shibata, *J. Electrochem. Soc.* **140**, 1131 (1993).
- ²J. Tao and N. W. Cheung, *IEEE Electron Device Lett.* **14**, 249 (1993).
- ³M. O. Abelfotoh and B. G. Stevansson, *Phys. Rev.* **44**, 12 742 (1991).
- ⁴A. Broniaowski, *Phys. Rev. Lett.* **62**, 3074 (1989).
- ⁵K. Holloway, P. M. Fryer, C. Cabral, Jr., J. M. E. Harper, and P. J. Bailey, *J. Appl. Phys.* **71**, 5433 (1992).
- ⁶P. Catania, J. P. Doyle, and J. J. Cuomo, *J. Vac. Sci. Technol. A* **10**, 3318 (1992).
- ⁷C. A. Chang, *J. Appl. Phys.* **67**, 7348 (1990).
- ⁸E. Kolawa, J. S. Chen, J. S. Reid, P. J. Pokela, and M.-A. Nicolet, *J. Appl. Phys.* **70**, 1369 (1991).
- ⁹C. A. Chang, *J. Appl. Phys.* **67**, 6184 (1990).
- ¹⁰S.-Q. Wang, S. Suthar, C. Hoeflich, and B. J. Burrow, *J. Appl. Phys.* **73**, 2301 (1993).
- ¹¹J. O. Olowolafe, J. Li, and J. W. Mayer, *J. Appl. Phys.* **68**, 6207 (1990).
- ¹²S.-Q. Wang, I. J. M. M. Raaijmakers, B. J. Burrow, S. Suthar, S. Redkar, and K. B. Kim, *J. Appl. Phys.* **68**, 5176 (1990).
- ¹³K. C. Park and K. B. Kim, *J. Electrochem. Soc.* (in press).
- ¹⁴A. Charai, H. E. Hornstrom, O. Thomas, P. M. Fryer, and J. M. E. Harper, *J. Vac. Sci. Technol. A* **7**, 784 (1989).
- ¹⁵R. E. Thomas, K. J. Guo, D. B. Aaron, E. A. Dobisz, J. H. Perepezko, and J. D. Wiley, *Thin Solid Films* **150**, 245 (1987).
- ¹⁶S.-Q. Wang, *MRS Bull.* Aug. (1994).
- ¹⁷*Binary Phase Diagram*, edited by T. B. Massalski (The Materials Information Society, Materials Park, 1990).
- ¹⁸B. Mehrotra and J. Stimmell, *J. Vac. Sci. Technol. B* **5**, 1736 (1987).
- ¹⁹S. Wolf and R. N. Tauber, *Silicon Processing for the VLSI Era* (Lattice Press, CA, 1987), Vol. 1, p. 533.
- ²⁰P. Catania, R. A. Roy, and J. J. Cuomo, *J. Appl. Phys.* **74**, 1008 (1993).
- ²¹L. A. Clevenger, A. Mutscheller, J. M. E. Harper, C. Cabral, Jr., and K. Barmak, *J. Appl. Phys.* **72**, 4918 (1992).
- ²²P. N. Baker, *Thin Solid Films* **14**, 3 (1972).
- ²³L. G. Feinstein and F. C. Livermore, *Thin Solid Films* **16**, 129 (1973).
- ²⁴A. Noya, K. Sasaki, and M. Takeyama, *Jpn. J. Appl. Phys.* **32**, 911 (1993).
- ²⁵M. H. Rottersman and M. J. Bill, *Thin Solid Films* **61**, 281 (1979).
- ²⁶J. S. Reid, E. Kolawa, R. P. Ruiz, and M.-A. Nicolet, *Thin Solid Films* **236**, 319 (1993).
- ²⁷X. Sun, E. Kolawa, J. S. Chen, J. S. Reid, and M.-A. Nicolet, *Thin Solid Films* **236**, 347 (1993).
- ²⁸R. E. Thomas, J. H. Perepezko, and J. D. Wiley, *Appl. Surf. Sci.* **26**, 534 (1986).
- ²⁹I. Barin, *Thermochemical Data of Pure Substances* (VCH, New York, 1989).